ARTICLE

A Trifluoromethyl-containing Pyrrolo[3,2-b]pyrrole Photoinitiator with Long Wavelength in Radical Photopolymerization under LED Irradiation

Congcong Liu[a], Yuanyuan Xu[b], Yukun Liu[a], Yu Chen[a*], Xiaoyuan Zhang[a], Jinghan Li[a], Ying Ma[a], Yaolong Li[c], Song Xue[a*]

a. Tianjin Key Laboratory of Organic Solar Cells and Photochemical Conversion, School of Chemistry and Chemical Engineering, Tianjin University of Technology, Tianjin 300384, China
b. School of Materials Science and Engineering, Tianjin University of Technology, Tianjin 300384, China
c. Tianjin Dage Technology Co., Ltd., Tianjin 301700, China

(Dated: Received on December 15, 2023; Accepted on April 29, 2024)

Pyrrolo[3,2-b]pyrrole is a good building block for radical photoinitiators. In this study, free-radical photoinitiator 1,4-bis(4-bromophenyl)-2,5-bis(4-(trifluoromethyl)phenyl)-1,4-dihydropyrrolo[3,2-b]pyrrole (PyBF), containing a symmetric trifluoromethyl (-CF_3) end group, is synthesized via a one-step aldehyde–ketone condensation reaction for light-emitting diode (LED) photopolymerization. The -CF_3 groups are incorporated into the 2,5-phenyl on the pyrrolo[3,2-b]pyrrole core. PyBF rapidly initiates the photopolymerization of acrylate prepolymers and monomers under LED illumination at 365 and 405 nm. A possible photolysis mechanism is provided. In the presence of amines, PyBF increases the gel fraction rate of polyethylene glycol diacrylate (PEGDA) from 63.4% to 80.0%, indicating good potential as a two-component photoinitiator. PyBF exhibits a thermal decomposition temperature in an excess of 300 °C, comparable to that of a commercial photoinitiator (diphenyl(2,4,6-trimethylbenzoyl)phosphine oxide, TPO), indicating its thermal stability. PyBF shows low migration in light-curing materials. Scanning electron microscopy images indicate that the materials of the PyBF/TPO/PEGDA mixture cured using the PyBF/TPO two-component photoinitiator system exhibit a smooth surface, in contrast to those cured with PyBF/PEGDA and TPO/PEGDA systems. The cured materials also display low curing shrinkage. Therefore, the pyrrolo[3,2-b]pyrrole radical photoinitiator exhibits high photoactivity in visible-light photopolymerization reactions.

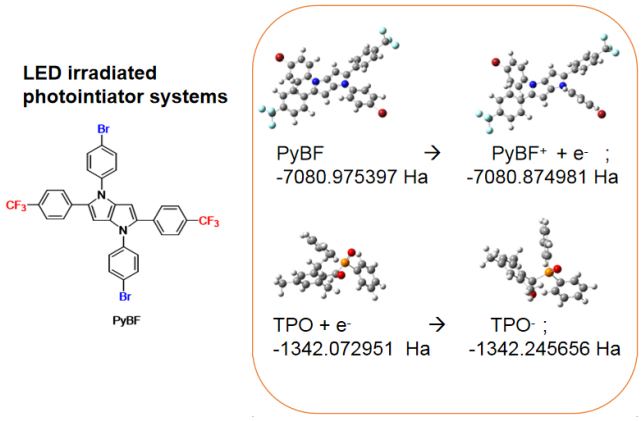

Key words: Photopolymerization, Photoinitiator, Pyrrolo[3,2-b]pyrrole, Amines, Trifluoromethyl groups, Visible light

I. INTRODUCTION

Photopolymerization is a light-induced reaction in which liquid monomers and prepolymers are converted to solid polymers in the presence of an appropriate pho-

* Authors to whom correspondence should be addressed.
E-mail: chenyu18417@email.tjut.edu.cn, xuesong@ustc.edu.cn

toinitiator [1–4]. Photopolymerization technology is economical, efficient, energy saving, enabling, and environment friendly [2, 5]. Owing to its unique technical advantages, photopolymerization is widely employed in coatings, inks, and adhesives. Furthermore, photopolymerization is crucial for advanced high-tech applications such as 3D printing [6], microelectronics [7], and biological materials [8]. Photoinitiators significantly influence the photopolymerization rate and performance of photopolymerized materials and are thus key components of photopolymerization reactions; however, photoinitiators with rapid initiation rates also require high thermal stability [9–12]. Heat-assisted light-curing 3D printing, which requires cured materials to achieve a high degree of curing and thermal stability to ensure strong mechanical properties, has recently surged in popularity [13]. Thus, photoinitiators with rapid initiation rates also require good thermal stability.

Radical photoinitiators absorb light in the ultraviolet (250–420 nm) or visible (400–800 nm) regions, generating free radicals that initiate the polymerization of monomers and form crosslinks between the resulting polymers [14, 15]. One-, two-, and multicomponent visible-light photoinitiators have proven suitable for current applications [16–22]. Radical photoinitiators based on conjugated skeletons such as carbazole [3, 17, 23–26], phenothiazine, and thioxanthone [5], exhibit broad absorption bands. The development of commercial photoinitiators for multicomponent visible-light photoinitiators has extensively broadened the practical applications of photopolymerization owing to the rapid photoinitiation rate and high photopolymerization conversion [27]. Commercial phosphine oxide, diphenyl(2,4,6-trimethylbenzoyl)phosphine oxide (TPO), is commonly employed upon light-emitting diode (LED) irradiation at 405 nm [28, 29].

Conjugated-skeleton photoinitiators have achieved remarkable results in multicomponent systems that typically comprise commercial cationic photoinitiators. Commercial cationic photoinitiators commonly absorb in the UV region, while the conjugated compounds absorb in the visible region; thus, these conjugated photoinitiators broaden the absorption and prevent the shrinkage of cured polymers owing to their rigid conjugated structure. Moreover, photoinitiator migration can be greatly reduced significantly using appropriately designed conjugated compounds. Amines are good co-photoinitiators for commercial photoinitiators. Xu *et al.* developed six ketone compounds as visible-light-sensitive photoinitiators in combination with an amine and iodonium salt for the free-radical polymerization of acrylates upon LED irradiation at 405 nm [30]. Deng *et al.* synthesized a series of bis-chalcone-based visible-light photoinitiators with redshifted maximum absorption wavelengths. A three-component system containing these photoinitiators with iodonium salt and an amine coating achieved a low migration ratio [31]. Zhu *et al.* developed homosubstituted thiazolothiazole-based photoinitiators coupled with one or two additives that exhibited outstanding photoinitiation abilities in both free-radical and cationic photopolymerization under 410 nm LED radiation with minor shrinkage [32]. Xue *et al.* combined a pyrrole-based enone dye that reacts with amines with a commercial iodonium salt [33]. Tang *et al.* developed a high-performance LED photoinitiator using conjugated 1,3-bis(1-methyl-1H-2-yl)prop-2-en-1-one with two pyrrole rings [34]. This photoinitiator possessed a high molar extinction coefficient, ranging from 365 nm to 425 nm, and initiated both cationic and free-radical photopolymerization in the presence of a commercial diphenyliodonium salt. Li *et al.* designed three novel Norrish II photoinitiators consisting of pyrrole chalcones with D-π-A structures. In combination with a common amine co-initiator, the excellent photochemical activity of these pyrrole chalcones effectively initiated the free-radical photopolymerization of acrylates under blue LED illumination, as demonstrated by the observed photopolymerization kinetics [35]. In a recent study, symmetric trifluoromethyl (-CF_3) groups were introduced into the pyrrolo[3,2-b]pyrrole core to produce an A–D–A molecular structure for radical photopolymerization. Amines improved the conversion rate of an acrylate resin containing PyBF, while the combination of TPO and PyBF improved the shrinkage resistance of the cured materials. Both the molar extinction coefficient and thermal decomposition temperature (T_d) of PyBF are higher than those of TPO, which enables the pyrrolo[3,2-b]pyrrole photoinitiator to be used under visible light conditions. Therefore, pyrrole and other five-membered heterocyclic rings are promising candidates for long-wavelength photopolymerization and exhibit high photoreaction activity with co-initiators and commercial photoinitiators.

Pyrrole is a five-membered heterocycle that has recently attracted attention as a promising framework for the design of photoinitiators owing to its facile chemical modification, low oxidation potential, and high thermal and chemical stabilities [33, 36]. Xue *et al.* achieved

DOI: 10.1063/1674-0068/cjcp2312131

high monomer conversions using symmetric bifunctional pyrrole-based dyes, which exhibited exceptional reactivity owing to the strength of intermolecular interactions and the generation of efficient initiating radicals [37]. These results demonstrate the utility of pyrrole groups as functional building blocks for radical photoinitiators. Li *et al.* developed a novel one-step synthetic route to a bifunctional pyrrole-carbazole-based photoinitiator that exhibited excellent absorption at 405 nm and the ability to donate hydrogen to sensitize commercial triarysulfonium salts, thereby extending the absorption window of onium salts to the visible-light region [38]. Rather than the -NO_2 groups of our previously reported photoinitiator with energy gaps between 2.4 and 2.9 eV owing to strong push–pull characteristics [39], the -CF_3 groups at the 2,5-phenyl and -Br at the 1,4-phenyl on the pyrrolo[3,2-b]pyrrole core of A–D–A in this work were identified as the substituents responsible for improving the photoinitiation ability of the pyrrolo[3,2-b]pyrrole photoinitiators upon LED irradiation at 405 nm.

In this study, we further investigated the 1,4-dihydropyrrolopyrroles developed by Gryko *et al.* [40, 41]. A photoinitiator, 1,4-bis(4-bromophenyl)-2,5-bis(4-(trifluoromethyl)phenyl)-1,4-dihydropyrrolo[3,2-b]pyrrole (PyBF), with symmetric bifunctional -CF_3 end groups, was synthesized via a one-step aldehyde–ketone condensation reaction. The visible-light initiation ability of PyBF, its relationship with different components, and the surface morphology of the corresponding cured materials were examined. PyBF was investigated as a one-component free-radical photoinitiator under LED lamps at 365 nm and 405, as well as for co-initiator with either amines or commercial photoinitiators (TPO) at 405 nm. Both acrylate prepolymers and monomers were employed in the photopolymerization formulations. The thermal stability of PyBF was compared with that of TPO. The surface morphologies of the cured materials from different photopolymerization systems containing PyBF were also examined using scanning electron microscopy (SEM). In summary, this pyrrole photoinitiator shows potential for rational design.

II. EXPERIMENTS

A. Materials

4-Trifluoromethylbenzaldehyde, 4-bromoaniline, 2, 3-butanedione, *p*-toluene sulfonic acid (TsOH), acetic acid (AcOH), and 2,4,6-trimethylbenzoyl diphenylphosphine oxide (TPO) were purchased from Energy Chemicals. The acrylate resins trimethylolpropane triacrylate (TMPTA) and polyethylene glycol acrylate (PEGDA) were purchased from Tokyo Chemical Industry.

B. Characterization

The nuclear magnetic resonance (NMR) spectra were recorded in deuterated chloroform ($CDCl_3$) with a Bruker AM-400 spectrometer (400 MHz for ^{1}H NMR and 100 MHz for ^{13}C NMR). Ultraviolet-visible measurements were performed using a SHIMADZU UV-2600 spectrometer. A HITACHI F-4500 fluorescence spectrometer was used to obtain fluorescence spectra. Cyclic voltammetry (CV) measurements were conducted using a CHI660D electrochemical workstation in a deoxygenated dichloromethane solution of tetrabutylammonium hexafluorophosphate (n-Bu_4NPF_6) under a nitrogen atmosphere (concentration of 0.1 mol/L). A glassy carbon dish (working electrode), platinum electrode (counter electrode), and Ag/AgCl electrode (reference electrode) were used. The measurements were performed using ferrocene as the standard. Thermogravimetric (TG) analyses were conducted using a DSC 200 F3 Maia (NETZSCH, Germany) at a heating rate of 10 °C/min under a nitrogen atmosphere. Mass spectrometry (Shimadzu, Japan) was used to study the photolysis of PyBF. The light source was an FUV-6BK UV curing machine connected to LED irradiators of 365 and 405 nm (Guangzhou Banwoo Electronic Technology Co., Ltd.). NIR spectroscopy was measured on a 5700 infrared spectrometer (Nicolet, USA). EPR experiments were carried out using a Bruker MicroESR.

C. Synthesis of PyBF

PyBF was synthesized following the original procedure developed by Gryko *et al.* [40]. The synthetic route of PyBF is shown in FIG. 1.

4-Trifluoromethylbenzaldehyde (1.007 g, 5.8 mmol), 4-bromoaniline (1.147 g, 6.7 mmol), and *p*-toluene sulfonic acid (0.287 g, 1.7 mmol) were placed in a two-necked bottle and stirred in 25 mL of acetic acid at 90 °C for 0.5 h. Then, butane-2,3-dione (0.127 g, 1.5 mmol) was added, and the resulting mixture was stirred at 90 °C for 3.5 h. After cooling, the precipitate was filtered and washed with acetic acid solution. The pure product was obtained via recrystallization from

DOI: 10.1063/1674-0068/cjcp2312131

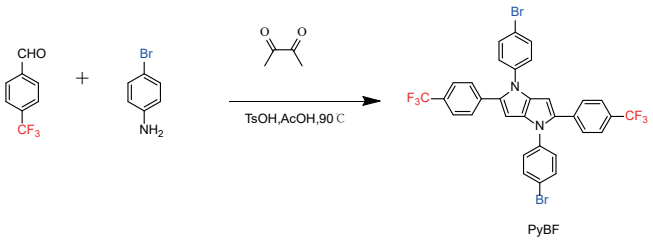

FIG. 1 Synthetic route to PyBF.

ethyl acetate, resulting in PyBF with the following characteristics. Light-yellow solid, 48% yield. ^{1}H NMR: (400 MHz, chloroform-d) δ=7.52 (m, 8H), δ=7.30 (d, J=8.80 Hz, 4H), δ=7.15 (d, J=8.80 Hz, 4H), δ=6.45 (s, 2H). ^{13}C NMR: (101 MHz, chloroform-d) δ=138.59, 136.45, 135.19, 132.78, 132.43, 128.31, 128.09, 126.85, 125.56, 125.52, 119.95, 77.36. HRMS(ESI) (m/z): $[M+H]^+$ calculated for $C_{32}H_{18}Br_2F_6N_2$, 701.9741; found: 701.4982.

D. Steady state photolysis

The maximum absorption peaks of PyBF and TPO were measured using a UV-Vis spectrophotometer. The concentration of PyBF in the dichloromethane solution was 5×10^{-6} mol/L in dichloromethane solution, and that of TPO was 1×10^{-4} mol/L. The solutions were irradiated at different time intervals using different LED light sources. The light intensities at 365 and 405 nm were 1.0 and 15 mW/cm^2, respectively.

E. Gel fraction

The degree of conversion of monomers and prepolymers was determined using the gel fraction method, which is a convenient method for measuring insoluble fractions, such as cross-linked or network polymers [42–44].

Formulations of PyBF(0.5 wt%)/PEGDA at 365 and 405 nm were used for gel fraction testing. The formulation of PyBF(0.5 wt%)/TMPTA at 405 nm was used to compare different resins. PyBF(0.5 wt%)/TPO/PEGDA with different weight ratios of TPO (1 wt% and 0.5 wt%) and TPO/PEGDA with different weight ratios of TPO (1 wt% and 0.5 wt%) were also examined to evaluate component interactions and compare the photoinitiation ability of PyBF. Blank glass sheets were numbered and weighed, and their measurements were recorded. Then, a sample of the photopolymerization system was dropped onto a glass sheet, and its weight was recorded as m_1. An LED lamp was used to irradiate the samples at regular intervals. After irradiation, the glass sheets were sufficiently immersed in an ethanol solution and placed in an oven to dry to a constant weight. The remaining solid weight was recorded as m_2. The gel fraction rate was calculated according to the following (Eq.(1)).

$$\omega = \frac{m_2}{m_1} \times 100\% \tag{1}$$

Formulations of PyBF(0.5 wt%)/triethylamine (TEA)/PEGDA and PyBF/*N*-methylpyrrolidone (NMP)/PEGDA were also prepared to further investigate the interactions in these two-component photoinitiation systems. The amount of TEA and NMP was kept at 150 μL.

F. Near infrared (NIR) spectroscopy tests

NIR spectroscopy was used for monitoring the photopolymerization samples to detect the characteristic absorption peak change of the C=C double bond group for acrylate resins with illumination time. The prepared sample was placed in a plastic round-hole mold with a diameter of 6 mm. An average value was determined from three repeated NIR tests. The double bond conversions of acrylate resins were calculated by detecting the characteristic absorption peak of C=C double bond groups at 6170 cm^{-1}, as follows:

$$\text{Conversion}/\% = \left(1 - \frac{S_t}{S_0}\right) \times 100\% \tag{2}$$

where S_t is the area of the C=CH characteristic absorbance peak, and S_0 is the initial area of the C=CH characteristic absorbance peak [45].

G. Electron paramagnetic resonance (EPR) detection

The radicals were generated at room temperature upon the LED irradiator of 405 nm exposure. In EPR spin trapping experiments, the experimental parameters were set and the radicals were trapped by phenyl-ntertbutylnitrone (PBN) [39]. The microwave power was 15 mW with a frequency of 9714.4 MHz.

III. RESULTS AND DISCUSSION

A. Synthesis

PyBF was synthesized via a one-pot reaction and easily purified through recrystallization. The corresponding ^{1}H and ^{13}C NMR spectra are shown in FIG. S1 in Supplementary materials (SM).

DOI: 10.1063/1674-0068/cjcp2312131

B. Spectroscopic properties, TG, and theoretical calculations

The UV absorption spectra of the two photoinitiators (PyBF and TPO) were measured, as they were expected to match well with LED light sources of different wavelengths. The corresponding absorption spectra are shown in FIG. 2(a). PyBF exhibits two main absorption bands at approximate 256 and 368 nm. The main absorption band of PyBF matches well with the near-UV and visible light range of 350–420 nm. PyBF is a promising pyrrolo[3,2-b]pyrrole-based photoinitiator for applications in LED photopolymerization at 405 nm. The corresponding PyBF and TPO concentrations were 5×10^{-6} and 1×10^{-4} mol/L, respectively. TPO is a commercial radical photoinitiator, and its maximum absorption wavelength (λ_{max}^{abs}) was determined to be at 295 nm. The maximum molar extinction coefficients of PyBF and TPO are 292200 and 1640 $mol\cdot L^{-1}\cdot cm^{-1}$, respectively. The maximum emission wavelengths (λ_{max}^{fl}) of PyBF and TPO were also determined to be 424 and 460 nm at a concentration of 1×10^{-4} mol/L (FIG. 3 (a) and (b)).

The thermal properties of PyBF and TPO were determined through TG [46]. The temperature range of the weight loss curves is from 25 °C to 550 °C. FIG. 2(b) shows the weight loss curves of PyBF and TPO. The decomposition temperatures (T_d) of PyBF and TPO are 340.5 and 295 °C, respectively. The thermal stability of PyBF is sufficient for storage and processing. The new photoinitiator with -CF_3 exhibits T_d values higher than 200 °C, indicating the good heat resistance of PyBF based on the pyrrolo[3,2-b]pyrrole core.

Quantum chemical calculations of the electronic properties and geometries of PyBF were performed using DFT at the B3LYP/6-31G level [47]. All structural optimizations and energy calculations were performed using the GAUSSIAN 09 software. The frontier orbitals of PyBF and the electrostatic potential (ESP) surface profile for PyBF are shown in FIG. 2(c). The ESP results show that the inductive effect of the electron-withdrawing groups caused a negative charge to form on the -CF_3 groups. In particular, the charge distribution of the pyrrolo[3,2-b]pyrrole core on PyBF is negative, indicating the electron-rich property of pyrrolo[3,2-b]pyrrole. The highest occupied molecular orbital (HOMO) of PyBF is mainly located between pyrrolo[3,2-b]pyrrole and 2,5-diphneyl containing -CF_3, whereas the lowest unoccupied molecular orbital (LUMO) is almost delocalized over the entire molecule. The singlet excited state energy (E_{00}) value calculated from the optical results is 3.09 eV for PyBF.

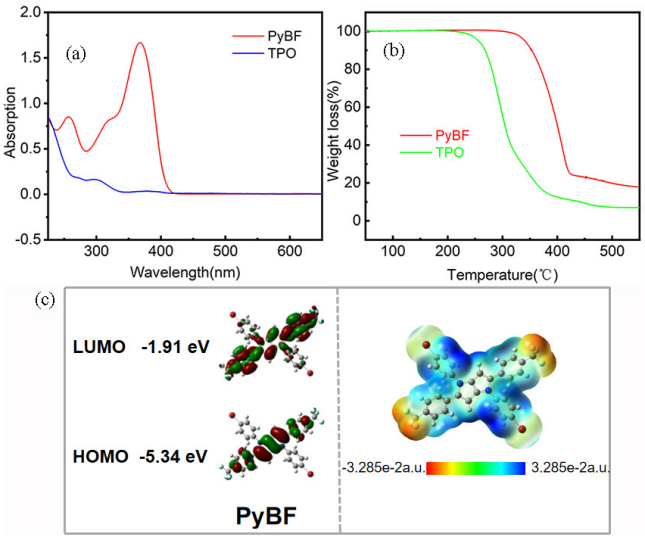

FIG. 2 (a) UV-Vis absorption spectra of PyBF and TPO in dichloromethane; (b) TG curves of PyBF and TPO; (c) DFT calculations of the frontier molecular orbitals of PyBF and the electrostatic potential (ESP) surface profile of PyBF.

C. Photopolymerization systems with PyBF as radical photoinitiator

The gel fraction method was used to directly compare the curing conversions of the PyBF(0.5 wt%)/PEGDA system under LED lamps of 365/405 nm and PyBF(0.5 wt%)/TMPTA, as compared with TPO(0.5 wt%)/PEGDA system under LED lamps of 405 nm. FIG. 4(a) shows the effects of the irradiation wavelength on the photoinitiation ability of the pyrrolo[3,2-b]pyrrole-based radical photoinitiator. FIG. 4(b) shows the difference in the gel fractions of bifunctional acrylate prepolymer PEGDA and tri-functional acrylate monomer TMPTA induced by PyBF, as compared with TPO(0.5 wt%)/PEGDA system under LED lamps of 405 nm. The highest gel fraction rate of PEGDA/PyBF under 405 nm with a value beyond 60%, and that of commercial PEGDA/TPO is 100%. NIR results for PEGDA and TMPTA photoinitiated by PyBF are presented in FIG. S2 (SM). The procedure details have been provided in Section II.F. The double bond conversions of PEGDA/PyBF and TMPTA/PyBF are 55.7% and 33.8%, respectively. EPR spectrum was explored under 405-nm LED for

DOI: 10.1063/1674-0068/cjcp2312131

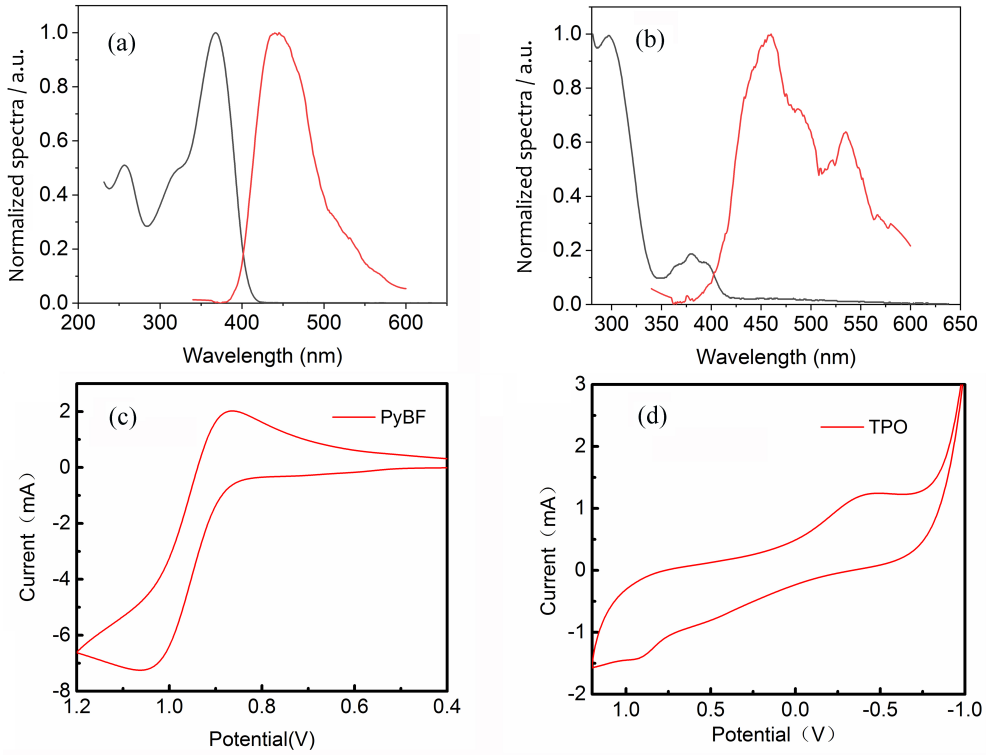

FIG. 3 Normalized absorption and emission spectra of (a) PyBF and (b) TPO, and CV curves of (c) PyBF and (d) TPO in dichloromethane.

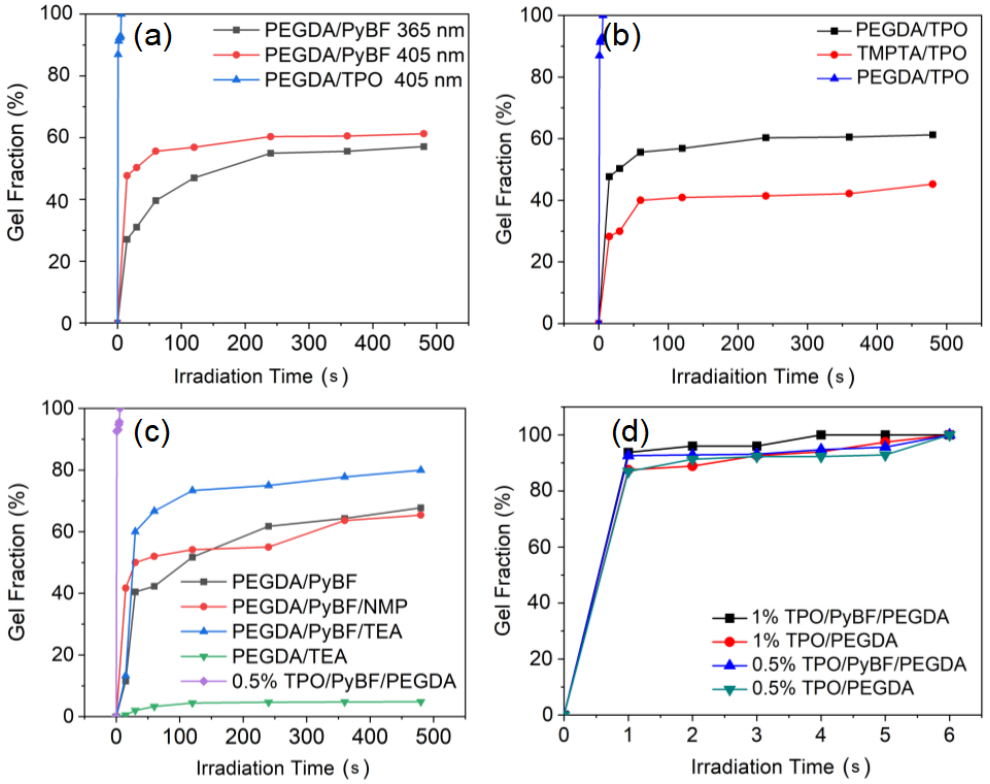

FIG. 4 Gel fractions of (a) samples PEGDA/PyBF after irradiation at 365 and 405 nm, compared with PEGDA/TPO irradiated at 405 nm, (b) samples of PEGDA/PyBF, TMPTA/PyBF, and PEGDA/TPO, (c) PEGDA/PyBF, PEGDA/PyBF/NMP, PEGDA/PyBF/TEA, PEGDA/TEA, and 0.5%TPO/PyBF/PEGDA, and (d) samples of PyBF (0.5 wt%)/TPO(1 wt%)/PEGDA, TPO(1 wt%)/PEGDA, PyBF(0.5 wt%)/TPO(0.5 wt%)/PEGDA, and TPO(0.5 wt%)/PEGDA upon 405 nm irradiation.

DOI: 10.1063/1674-0068/cjcp2312131

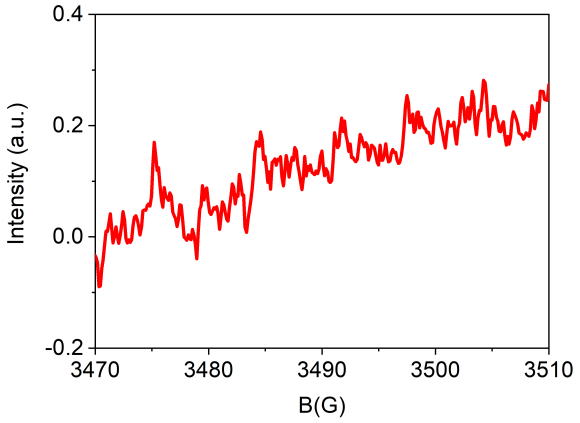

FIG. 5 EPR spectra obtained after the irradiation of a solution of PyBF/PBN upon the LED irradiator of 405 nm exposure for 240 s.

240 s, as shown in FIG. 5. The EPR signals reflect active free radicals generated through this pyrrolo[3,2-b]pyrrole photoinitiator. To enhance the polymerization performance of the curing system, triethylamine (TEA) and *N*,*N*-methylpyrrolidone (NMP) were added to the formulations, in which PyBF and PEGDA serve as the photoinitiator and curing resin, respectively [48]. Upon the addition of TEA, the gel fraction rate increased from 64.3% to 80.0%, whereas the addition of NMP increased the final conversion to only 65.4% (FIG. 4(c)). FIG. 4(c) also indicates TEA itself barely can initiate the polymerization of PEGDA. These experiments show that PyBF can function as both a one-component photoinitiator and as a two-component photoinitiator with amines under 405 nm irradiation. In these systems, PyBF has a weight ratio of 0.5 wt%, and thus the conversion of TPO(0.5 wt%)/PyBF/PEGDA system based on TPO(0.5 wt%)/PyBF two-component photoinitiator was used for comparison.

To further expand the application scope of pyrrolo[3,2-b]pyrrole photoinitiators, we combined PyBF with commercial visible-light radical photoinitiators. The corresponding gel fraction curves as a function of irradiation time are shown in FIG. 4(d). The absorption of commercial TPO aligns well with the 405 nm light source used in light-curing 3D printing technology for additive manufacturing. The final gel fraction rates of the PyBF(0.5 wt%)/TPO(1 wt%)/PEGDA and TPO(1 wt%)/PEGDA systems were 100%, whereas those at 1 s were 93.8% and 87.5%, respectively. With the addition of 0.5 wt% TPO, PyBF(0.5 wt%)/TPO(0.5 wt%)/PEGDA achieved a maximum gel fraction rate of nearly 100%, with rates of 92.6% and 87.5% at 1 s, respectively.

It is well known that too fast photopolymerization process will lead to large shrinkage. Applications in biomaterials and composite materials such as food packaging and medical materials require to reduce the potential risk of residual photoinitiators migrating from cured films [49, 50]. FIG. 6 compares the shrinkage and migration in photopolymerization systems photoinitiated by PyBF with commercial TPO, aiming to give a reasonable estimation of the properties of photopolymerized cured films in the presence of PyBF for future use. Results show the use of PyBF as a co-initiator alongside commercial photoinitiator improved the resistance to shrinkage [27, 32] and migration of the cured polymers [11, 31, 51]. FIG. 6(a)–(c) show the surface morphology images of the cured materials PyBF(0.5 wt%)/PEGDA, TPO(1 wt%)/PEGDA, and PyBF(0.5 wt%)/TPO (1 wt%)/PEGDA, respectively, observed using SEM. The cured materials of the three photopolymerization systems were prepared under a 405 nm LED lamp with a light intensity of 15 mW/cm^2 for 480 s. When the curing system was PyBF(0.5 wt%)/PEGDA, the surface exhibited an uneven and moderately textured morphology (FIG. 6(a)). As shown in FIG. 6(b), clear folds can be observed on the surface of the samples polymerized with TPO(1 wt%)/PEGDA. As shown in FIG. 6(c), the sample obtained using PyBF(0.5 wt%)/TPO(1 wt%)/PEGDA exhibits a flat and smooth surface with no wrinkles or folds, indicating low curing shrinkage after polymerization over the same duration.

To investigate the migration properties, the cured materials were weighed and soaked in 3 mL of acetonitrile. FIG. 6 (d) and (e) show the changes in absorption spectra at $\lambda_{\max}^{\text{abs}}$ with increasing soaking time for PyBF(0.5 wt%)/PEGDA and TPO(1 wt%)/PEGDA, respectively. FIG. 6(f) shows the changes in absorbance at the maximum absorption wavelengths after the cured film was soaked in acetonitrile for one day. Table S1 (SM) summarizes the migration ratios and weights of PyBF and TPO extracted from the cured materials. The migration ratio and extraction weight were calculated using Eq.(3) [52] and Eq.(4) [53], respectively.

$$\text{Migration ratio} = \frac{A \cdot M \cdot V_{\text{solution}}}{\varepsilon \cdot b \cdot m_0} \tag{3}$$

$$m = M \cdot c \cdot V = \frac{M \cdot A}{\varepsilon \cdot l} \times 3 \times 10^{-3} \tag{4}$$

The migration ratio of PyBF is similar to that of com-

DOI: 10.1063/1674-0068/cjcp2312131

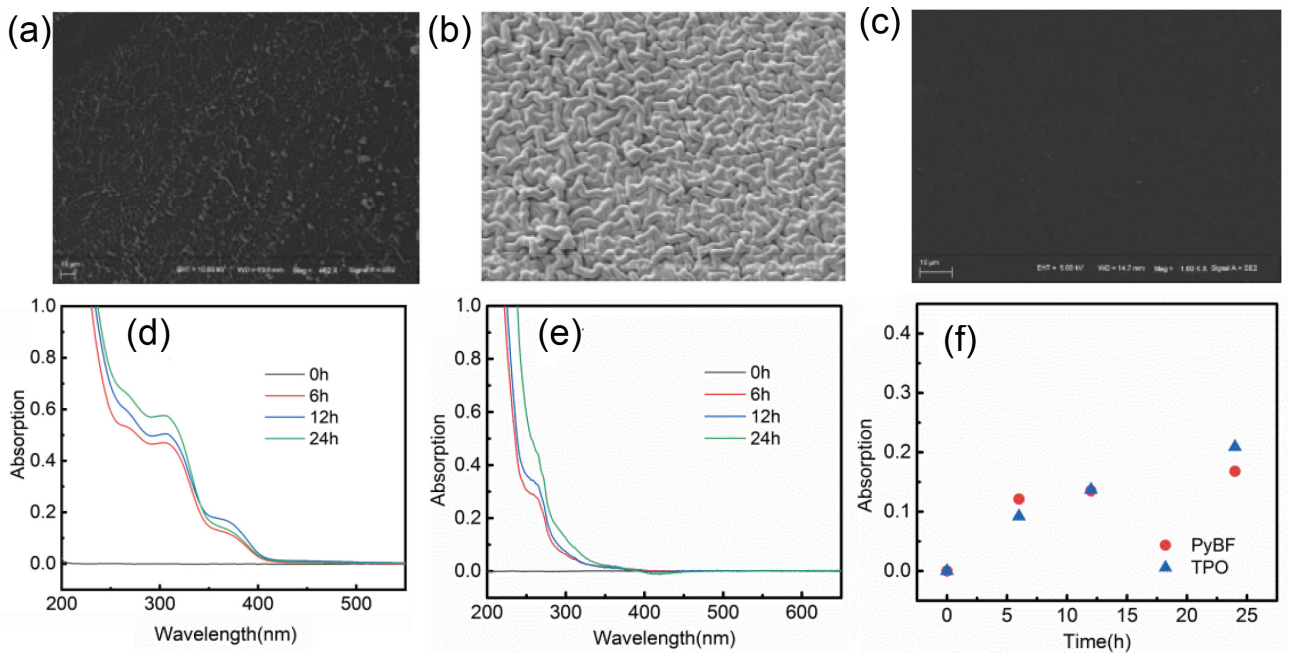

FIG. 6 SEM images showing the surface morphology of different curing systems: (a) PyBF/PEGDA, (b) TPO/PEGDA, and (c) PyBF/TPO/PEGDA. UV absorption spectra of the cured films of (d) PyBF(0.5 wt%)/PEGDA and (e) TPO (1 wt%)/PEGDA in acetonitrile. (f) Absorbances of PyBF and TPO at λ_{max}^{abs} corresponding to different soaking times in the cured materials.

mercial TPO (Table S1 in SM). The concentration of the photoinitiators was calculated from the absorption of the leaching solution at λ_{max}^{abs}. Low leaching of photoinitiator compounds enhances the hardness of cured films [28, 31]. The molecular weight of PyBF (704.3 g/mol) is larger than that of commercial TPO (348.4 g/mol).

The free energy change (ΔG_{el}) of the photoelectron reaction between the excited state of PyBF as the electron donor and TPO as the electron acceptor was calculated using the Rehm–Weller equation (Eq.(5)) [38].

$$\Delta G_{el} = E_{ox}\left(\frac{D}{D^{\bullet+}}\right) - E_{red}\left(\frac{A^{\bullet-}}{A}\right) - E_{00} \qquad (5)$$

The synergistic effect of TPO and PyBF is evident in the spectral and electrochemical behaviors of the PyBF/TPO two-component systems. The E_{00} of PyBF was calculated as 3.09 eV, based on the intersection wavelength of its absorption spectrum and emission spectrum using the formula $E_{00}= hcN/\lambda$. The CV results show the oxidation potential (E_{ox}) of the electron donor (PyBF) and the reduction potential (E_{red}) of the electron acceptor (TPO). In a separate experiment (FIG. 3 (c) and (d)), the oxidation potential of PyBF was determined to be 0.864 V, while the reduction potential of TPO was −0.910 V. The calculated ΔG_{el} of the

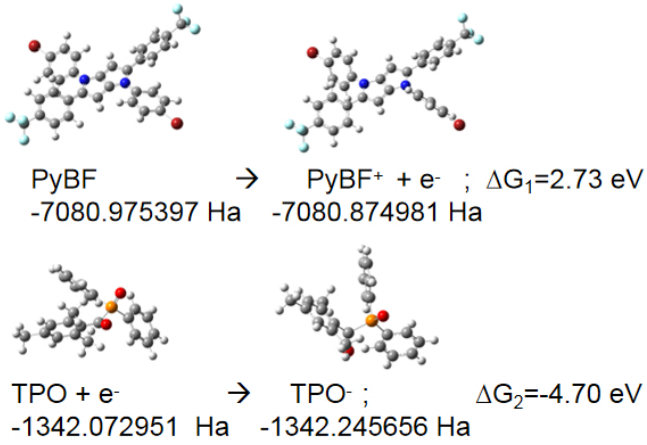

FIG. 7 DFT calculation on free energy changes of PyBF and TPO.

PyBF/TPO pair is −3.14 eV, indicating that the photoelectron transfer between the excited states of PyBF and TPO is thermodynamically allowed. This negative free energy change for the PyBF/TPO pair favors photoelectron-transfer reactions. DFT calculations were carried out with the B3LYP functional and the 6-31G basis set using the program Gaussian 09 [54]. The theoretical free energy change of charge transfer reaction between donor (PyBF) and acceptor (TPO) is to be a negative value of −1.97 eV, which is the sum of ΔG_1 and ΔG_2 (FIG. 7).

DOI: 10.1063/1674-0068/cjcp2312131

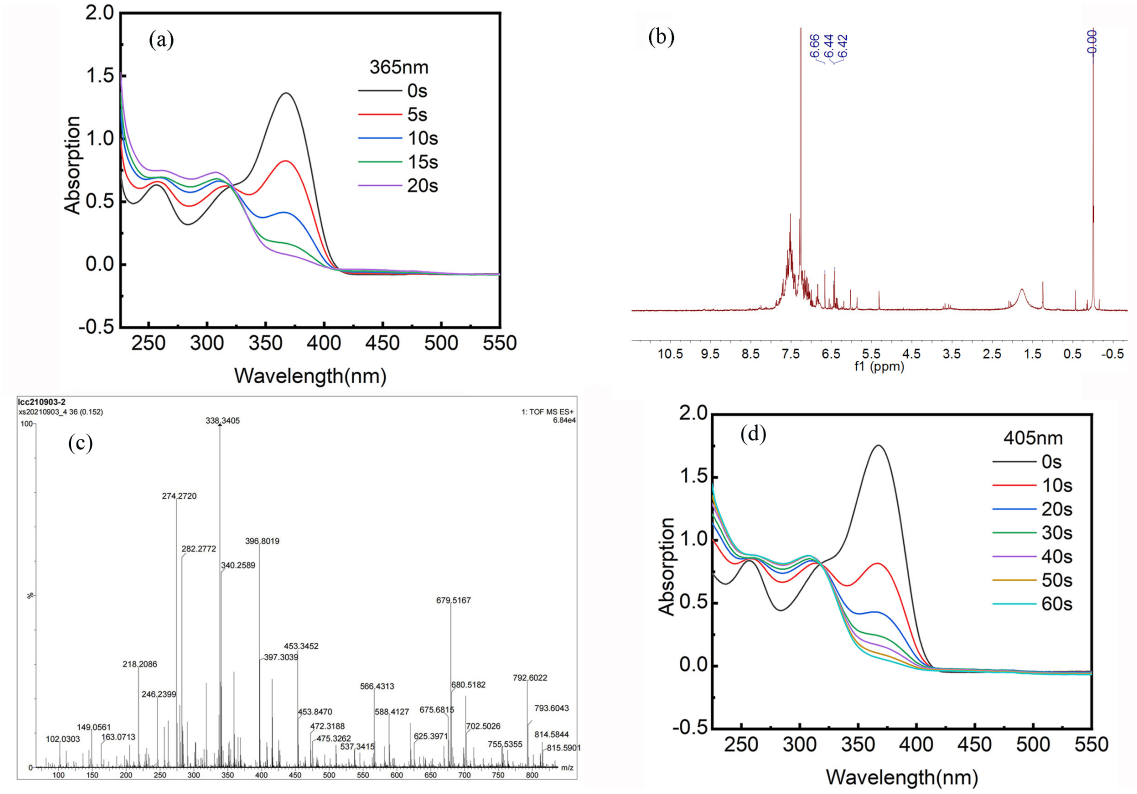

FIG. 8 (a) UV absorption spectra of PyBF at various illumination times upon LED irradiation at 365 nm. (b) ^{1}H NMR spectrum of PyBF in $CDCl_3$ after irradiation for 480 s. (c) Mass spectrum of PyBF after irradiation for 480 s. (d) UV absorption spectra of PyBF at various illumination times upon 405 nm LED irradiation.

D. Steady-state photolysis results

The photochemical reactions of PyBF were investigated using steady-state photolysis experiments [55, 56]. As shown in FIG. 8(a), the photolysis of individual PyBF molecules at 365 nm was highly efficient, achieving complete conversion within 60 s. The intensity of the main absorption band of PyBF at 368 nm continuously decreased upon irradiation. The appearance of new shoulder bands at 250–350 nm suggests that a new intermediate with blue-shifted absorption was generated upon the decomposition of the D–A structure, which is consistent with the results of our previous study [39]. The NMR and mass spectra also indicate that photolysis occurred during light irradiation. The ^{1}H NMR spectra obtained after irradiation are shown in FIG. 8(b). The characteristic peaks in the ^{1}H NMR spectrum of PyBF gradually changed after light exposure. As shown in FIG. S1(a) (SM), the chemical shift of PyBF at δ=6.46 ppm was attributed to the C–H groups of the pyrrolo[3,2-b]pyrrole structure. New peaks appeared at approximately 6.66 ppm after 480 s irradiation at 365 nm using the LED lamp, indicating that a new pyrrolo[3,2-b]pyrrole structure was formed during light irradiation. The mass spectra of PyBF acquired before and after photolysis upon irradiation using the LED light at 365 nm for 480 s are shown in FIG. S3 (SM) and FIG. 8(c), respectively. The mass spectrum obtained before photolysis exhibits a peak at m/z=701, corresponding to the exact mass of PyBF. After photolysis, a peak was observed at m/z=566, indicating the formation of a new structure. The peak at m/z=566 may correspond to the photolysis product, whose structure is shown in the schematic of the mechanism in FIG. 9, which suggests the cleavage of the C–C bond between the phenyl and -CF_3 groups after light irradiation. Amines react with the free radicals originated from PyBF to produce amine radicals, which can continue to produce active radicals even if there is oxygen on the surface according to reports [38, 57, 58]. Therefore, this may be the reason why the curing speed can be improved. Our results are consistent with the reports. The efficient photolysis of PyBF under an LED lamp at 405 nm (FIG. 8(d)) demonstrates its high photoreaction activity under visible light.

DOI: 10.1063/1674-0068/cjcp2312131

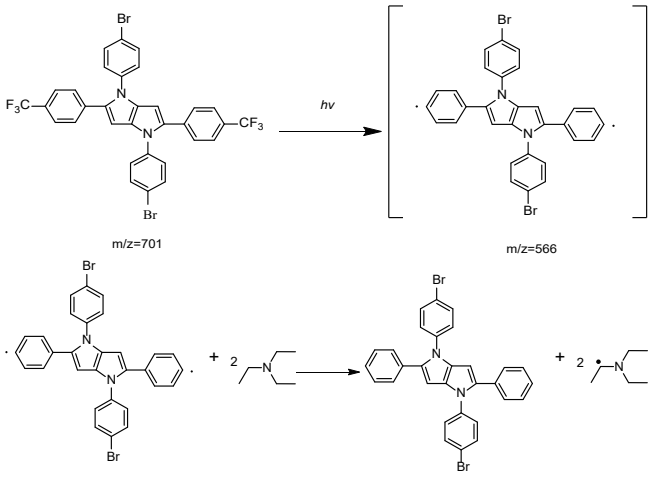

FIG. 9 Schematic of the mechanism of PyBF photolysis and that in corporation with TEA.

IV. CONCLUSION

Photoinitiator 1,4-bis(4-bromophenyl)-2,5-bis(4-(trifluoromethyl)phenyl)-1,4-dihydropyrrolo[3,2-b]pyrrole (PyBF), which features symmetric trifluoromethyl end groups, was synthesized via a one-step aldehyde–ketone condensation reaction. The effect of the symmetric -CF_3 moieties on the visible-light initiation ability, relationships with different parameters, and the surface morphology of the cured materials were examined. PyBF was investigated as a one-component free-radical photoinitiator upon irradiation using 365 nm and 405 nm LED lamps, and its applicability as a two-component photoinitiator alongside with TEA, NMP, and TPO upon irradiation at 405 nm was evaluated. The photopolymerization formulations contained both prepolymers and monomers. The thermal stability of PyBF was similar to that of commercial TPO. The PyBF/PEGDA system achieved a curing conversion of approximate 60%. The analyses of the gel fractions of PyBF/TEA/PEGDA indicate that the presence of TEA increased the curing conversion to >80%. Similarly, PyBF/TPO/PEGDA achieved a conversion of ~100%. Moreover, the SEM images revealed a surface morphology exhibiting a synergistic effect between PyBF and TPO. The negative ΔG_{el} value indicated that the photoelectron transfer between the excited state of PyBF and TPO is thermodynamically allowed. This pyrrole derivative will expand the functionality of photoinitiators, offering distinct absorption characteristics, photophysical properties, and interactions among the components of photoinitiation systems.

Supplementary materials: NMR spectra, the C=C double bond conversions as a function of irradiation time, mass spectra, and data of the leaching experiments.

V. NOTES

The authors have no relevant financial interests to declare.

VI. ACKNOWLEDGEMENTS

The authors gratefully thank for the financial support of the Tianjin Technical Expert Project (22YDTPJC00620).

[1] D. S. Esen, N. Arsu, J. P. Da Silva, S. Jockusch, and N. J. Turro, J. Polym. Sci. A: Polym. Chem. **51**, 1865 (2013).
[2] Y. Zhu, L. Li, Y. C. Zhang, Y. Ou, J. Y. Zhang, Y. Yagci, and R. Liu, Prog. Org. Coat. **174**, 107272 (2023).
[3] F. Dumur, Eur. Polym. J. **165**, 110999 (2022).
[4] D. Zhao, M. Z. Wang, Q. C. Wu, X. Zhou, and X. W. Ge, Chin. J. Chem. Phys. **27**, 607 (2014).
[5] X. D. Guo, H. Y. Zhou, and J. X. Wang, Prog. Org. Coat. **154**, 106214 (2021).
[6] T. T. Zhao, R. Yu, W. Huang, W. Zhao, and G. Wang, Polym. Adv. Technol. **32**, 980 (2021).
[7] S. X. Chen, C. Qin, M. Jin, H. Y. Pan, and D. C. Wan, J. Polym. Sci. **59**, 578 (2021).
[8] H. Y. Quan, T. Zhang, H. Xu, S. Luo, J. Nie, and X. Q. Zhu, Bioact. Mater. **5**, 110 (2022).
[9] G. Temel, N. Arsu, and Y. Yagci, Polym. Bull. **57**, 51 (2006).
[10] B. Seidl and R. Liska, Macromol. Chem. Phys. **208**, 44 (2007).
[11] W. W. Qiu, J. Z. Zhu, K. Dietliker, and Z. Q. Li, ChemPhotoChem **4**, 5296 (2020).
[12] F. Dumur, Eur. Polym. J. **178**, 111500 (2022).
[13] X. Kuang, Z. A. Zhao, K. J. Chen, D. N. Fang, G. Z. Kang, and H. J. Qi, Macromol. Rapid Commun. **39**, 1700809 (2018).
[14] H. W. Lai, D. Zhu, and P. Xiao, Macromol. Chem. Phys. **220**, 1900315 (2019).
[15] Y. Y. Bao, Macromol. Rapid Commun. **43**, 2200202 (2022).
[16] K. Sun, Y. Y. Xu, F. Dumur, F. Morlet-Savary, H. Chen, C. Dietlin, B. Graff, J. Lalevée, and P. Xiao, Polym. Chem. **11**, 2230 (2020).
[17] M. Y. Li, B. H. Bao, J. You, Y. Du, D. X. Li, H. T. Zhan, L. H. Zhang, and T. Wang, Prog. Org. Coat.

173, 107217 (2022).
[18] W. Liao, Q. Y. Liao, Y. Xiong, Z. Li, and H. D. Tang, J. Photochem. Photobiol. A **435**, 114297 (2023).
[19] M. Topa, E. Hola, M. Galek, F. Petko, M. Pilch, R. Popielarz, F. Morlet-Savary, B. Graff, J. Lalevée, and J. Ortyl, Polym. Chem. **11**, 5261 (2020).
[20] A. Balcerak, D. Kwiatkowska, and J. Kabatc, Polym. Chem. **13**, 220 (2022).
[21] T. B. Cavitt, C. E. Hoyle, V. Kalyanaraman, and S. Jönsson, Polymer **45**, 1119 (2004).
[22] A. Balcerak, D. Kwiatkowska, K. Iwińska, and J. Kabatc, Polym. Chem. **11**, 5500 (2020).
[23] C. Xu, S. Gong, X. Wu, Y. W. Wu, Q. Y. Liao, Y. Xiong, Z. Li, and H. D. Tang, Dyes Pigments **198**, 110039 (2022).
[24] A. A. Mousawi, A. Arar, M. Ibrahim-Ouali, S. Duval, F. Dumur, P. Garra, J. Toufaily, T. Hamieh, B. Graff, D. Gigmes, J. P. Fouassier, and J. Lalevée, Photochem. Photobiol. Sci. **17**, 578 (2018).
[25] F. Dumur, Eur. Polym. J. **175**, 111330 (2022).
[26] P. Hu, W. W. Qiu, S. Naumov, T. Scherzer, Z. Y. Hu, Q. D. Chen, W. Knolle, and Z. Q. Li, ChemPhotoChem **4**, 224 (2020).
[27] D. Manojlovic, M. D. Dramićanin, V. Miletic, D. Mitić-Ćulafić, B. Jovanović, and B. Nikolić, Dent. Mater. **33**, 454 (2017).
[28] Y. P. Wu, J. S. Ke, C. X. Dai, J. W. Wang, C. G. Huang, Y. Situ, and H. Huang, Eur. Polym. J. **175**, 111380 (2022).
[29] V. Miletic, P. Pongprueksa, J. De Munck, N. R. Brooks, and B. Van Meerbeek, J. Dent. **41**, 918 (2013).
[30] Y. Y. Xu, G. Noirbent, D. Brunel, F. Y. Liu, D. Gigmes, K. Sun, Y. J. Zhang, S. H. Liu, F. Morlet-Savary, P. Xiao, F. Dumur, and J. Lalevée, Eur. Polym. J. **132**, 109737 (2020).
[31] L. Deng and J. Q. Qu, Prog. Org. Coat. **174**, 107240 (2023).
[32] D. Zhu, X. Peng, P. Wagner, and P. Xiao, Dyes Pigments **206**, 110638 (2022).
[33] T. L. Xue, Y. Li, L. Q. Tang, R. F. Tang, J. Nie, and X. Q. Zhu, Dyes Pigments **191**, 109372 (2021).
[34] L. Q. Tang, J. Nie, and X. Q. Zhu, Polym. Chem. **11**, 2855 (2020).
[35] J. F. Li, H. Zheng, H. W. Lu, J. Y. Li, L. Yao, Y. J. Wang, X. J. Zhou, J. Nie, X. Q. Zhu, and Z. C. Fu, Eur. Polym. J. **176**, 111393 (2022).
[36] F. Dumur, Eur. Polym. J. **173**, 111254 (2022).
[37] T. L. Xue, L. Q. Tang, R. F. Tang, Y. Li, J. Nie, and X. Q. Zhu, Dyes Pigments **188**, 109212 (2021).
[38] Y. Li, U. Shaukat, S. Schlögl, T. L. Xue, J. F. Li, J. Nie, and X. Q. Zhu, Eur. Polym. J. **182**, 111700 (2023).
[39] Y. Y. Xu, Y. Chen, X. G. Liu, and S. Xue, ACS Omega **6**, 20902 (2021).
[40] A. Janiga, E. Glodkowska-Mrowka, T. Stoklosa, and D. T. Gryko, Asian J. Org. Chem. **2**, 411 (2013).
[41] M. Krzeszewski, D. Gryko, and D. T. Gryko, Acc. Chem. Res. **50**, 2334 (2017).
[42] Y. Sanai, T. Ninomiya, and K. Arimitsu, Prog. Org. Coat. **151**, 106038 (2021).
[43] Y. C. Chen, Y. T. Kuo, and T. H. Ho, Photochem. Photobiol. Sci. **18**, 190 (2019).
[44] J. S. Kim, J. U. Hwang, D. Baek, H. J. Kim, and Y. Kim, J. Mater. Res. Technol. **10**, 1176 (2021).
[45] Y. Chen, X. Q. Jia, M. Q. Wang, and T. Wang, RSC Adv. **5**, 33171 (2015).
[46] B. Li, Y. Cai, X. Tian, X. Z. Liang, D. Li, Z. Zhang, S. J. Wang, K. P. Guo, and Z. K. Liu, J. Energy Chem. **62**, 523 (2021).
[47] R. C. Zhou, H. Y. Pan, D. C. Wan, J. P. Malval, and M. Jin, Prog. Org. Coat. **157**, 106306 (2021).
[48] A. Merlin, D. J. Lougnot, and J. P. Fouassier, Polym. Bull. **3**, 1 (1980).
[49] Y. Yuan, C. Li, R. J. Zhang, R. Liu, and J. C. Liu, Prog. Org. Coat. **137**, 105308 (2019).
[50] Y. Y. Xu, G. Noirbent, D. Brunel, Z. F. Ding, D. Gigmes, B. Graff, P. Xiao, F. Dumur, and J. Lalevée, Dyes Pigments **185**, 108900 (2021).
[51] R. Zhong, H. Hu, and Y. F. Zhou, Materials **14**, 5272 (2021).
[52] S. Q. Fang, Y. L. Pang, and Y. Q. Zou, Chin. J. Polym. Sci. **36**, 521 (2018).
[53] Y. Y. Liu, T. T. Wang, C. B. Xie, X. J. Tian, L. Song, L. Liu, Z. W. Wang, and Q. Yu, Prog. Org. Coat. **142**, 105603 (2020).
[54] L. Blancafort and A. A. Voityuk, Phys. Chem. Chem. Phys. **19**, 31007 (2017).
[55] Z. X. Tang, Y. J. Gao, S. L. Jiang, J. Nie, and F. Sun, Prog. Org. Coat. **170**, 106969 (2022).
[56] J. F. Li, J. Nie, and X. Q. Zhu, Prog. Org. Coat. **151**, 106099 (2021).
[57] C. G. Roffey, *Photopolymerization of Surface Coatings*, Chichester: Wiley, 353 (1982).
[58] Y. C. Chen, T. Y. Liu, and Y. H. Li, J. Coat. Technol. Res. **18**, 99 (2021).

DOI: 10.1063/1674-0068/cjcp2312131